

# Enhanced-Selectivity High-Linearity Low-Noise Mixer-First Receiver With Complex Pole Pair Due to Capacitive Positive Feedback

Yuan-Ching Lien<sup>ID</sup>, Student Member, IEEE, Eric A. M. Klumperink, Senior Member, IEEE, Bernard Tenbroek, Jon Strange, Senior Member, IEEE, and Bram Nauta, Fellow, IEEE

**Abstract**—A mixer-first receiver (RX) with enhanced selectivity and high dynamic range is proposed, targeting to remove surface acoustic-wave-filters in mobile phones and cover all frequency bands up to 6 GHz. Capacitive negative feedback across the baseband (BB) amplifier serves as a blocker bypassing path, while an extra capacitive positive feedback path offers further blocker rejection. This combination of feedback paths synthesizes a complex pole pair at the input of the BB amplifier, which is upconverted to the RF port to obtain steeper RF bandpass filter roll-off and reduced distortion. This paper explains the circuit principle and analyzes RX performance. A prototype chip fabricated in 45-nm partially depleted silicon on insulator (SOI) technology achieves high out-of-band linearity (input-referred third-order intercept point (IIP3) = 39 dBm and input-referred second-order intercept point (IIP2) = 88 dB) combined with sub-3-dB noise figure. Desensitization due to a 0-dBm blocker is only 2.2 dB at 1.4 GHz.

**Index Terms**—Bandpass, block rejection, CMOS, compression point, frequency-division duplex (FDD), high linearity, input-referred second-order intercept point (IIP2), input-referred third-order intercept point (IIP3), low noise, mixer first,  $N$ -path filter, passive mixer, receiver (RX), surface acoustic-wave (SAW) less, tunable, wideband.

## I. INTRODUCTION

TO IMPROVE data rate and capacity, cellular phones based on the long-term evolution (LTE) standard have to support an ever increasing number of bands. For 5G, a receiver (RX) covering much of the spectrum up to 6 GHz is likely required. The mobile RXs need to deal with large out-of-band (OOB) blockers, while frequency-division duplex (FDD) also introduces strong self-interference from the transmitter (TX). To prevent degradation in sensitivity, off-chip high-linearity surface acoustic-wave (SAW) filters are often adopted. However, these filters are not tunable, increase size and cost, and introduce 2–3 dB in-band loss, making

Manuscript received August 29, 2017; revised November 6, 2017 and December 22, 2017; accepted December 23, 2017. Date of publication February 5, 2018; date of current version April 23, 2018. This paper was approved by Guest Editor Danilo Manstretta. (Corresponding author: Yuan-Ching Lien.)

Y.-C. Lien, E. A. M. Klumperink, and B. Nauta are with the IC Design Group, University of Twente, 7500 AE Enschede, The Netherlands (e-mail: y.lien@utwente.nl).

B. Tenbroek and J. Strange are with the RF Department, Mediatek, Kent ME19, U.K.

Color versions of one or more of the figures in this paper are available online at <http://ieeexplore.ieee.org>.

Digital Object Identifier 10.1109/JSSC.2018.2791490

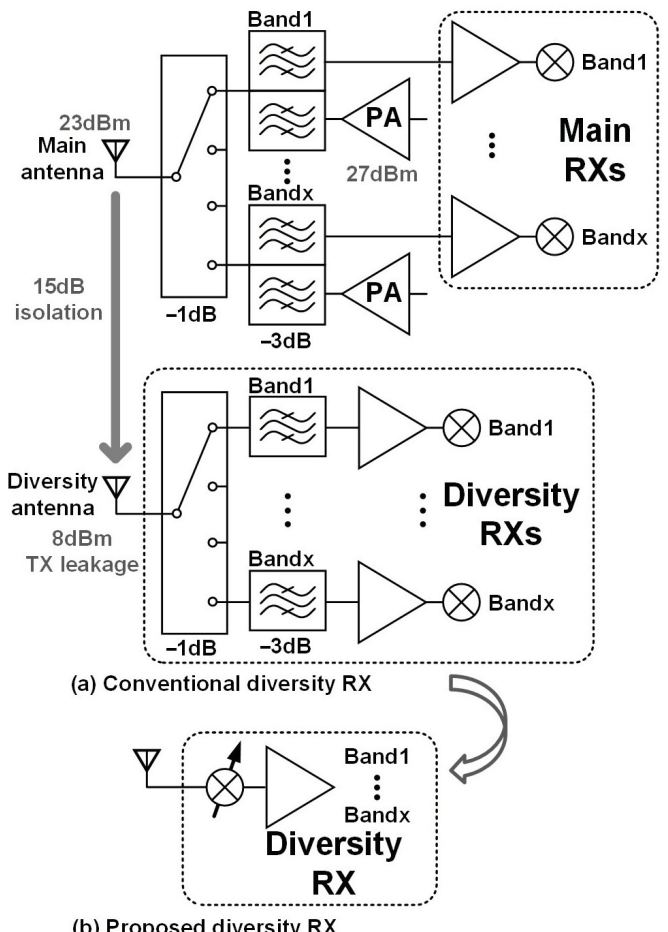


Fig. 1. (a) Conventional LTE RX with external SAW filters. (b) Proposed single tunable diversity RX without external SAW filters.

multi-band 1–6 GHz support troublesome. SAW-less solutions compatible with CMOS integration are highly desired.

Antenna diversity with two antennas is widely applied in modern cellular phones to improve the quality and reliability of wireless links. Moreover, two or even more receive antennas are wanted for multi-in multi-out. In this paper, we focus on a diversity antenna RX for a conventional FDD cellular system as shown in Fig. 1(a).

The typical TX power is as strong as +27 dBm, and there is about 15-dB isolation from the main antenna to the diversity antenna. Including TX filter and switch losses,

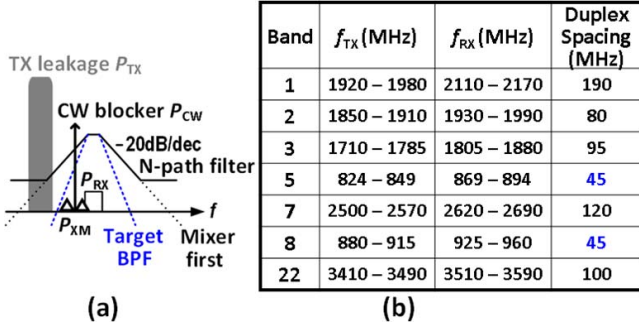


Fig. 2. (a) Related target-BPF profile. (b) Some LTE frequency bands.

about +23 and +8 dBm TX leakage, are present at the RF input ports of the main and diversity RXs, respectively. Usually, SAW RX filters [see Fig. 1(a)] provide TX-RX isolation to relax the RX linearity requirements to a feasible level. Targeting more integration, recent work has shown that passive switch-capacitor  $N$ -path filtering with tunable center frequency in mixer-first RXs can achieve >10-dBm blocker 1-dB compression point (B1dB) and a good input-referred third-order intercept point (IIP3) of 20–30 dBm [1]–[3]. This shows promise to remove the off-chip SAW filters in the diversity RX and also reduce the number of diversity RXs to a single one, as shown in Fig. 1(b). This paper explores the feasibility of such a RX in CMOS.

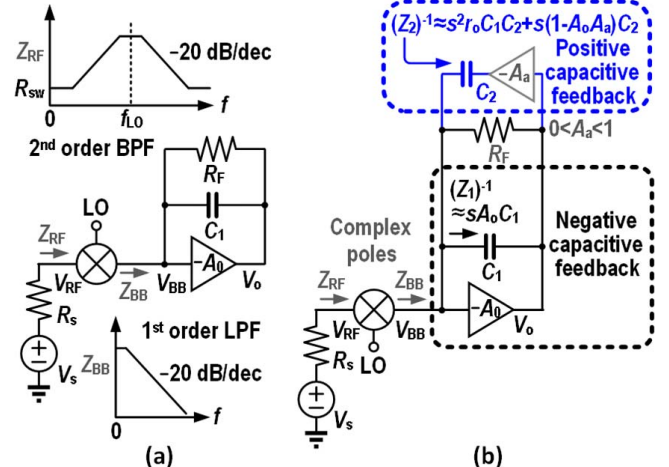
In an FDD system, cross-modulation due to TX leakage and an in-band continuous-wave (CW) blocker deteriorates RX sensitivity, which can be related to an IIP3 requirement [4], [5]

$$\text{IIP3} = \frac{P_{CW} + 2P_{TX} - P_{XM} - 5}{2}. \quad (1)$$

As shown in Fig. 2(a),  $P_{CW}$  is the power of the CW blocker (typically –40 dBm),  $P_{TX}$  is the TX leakage (8 dBm),  $P_{XM}$  is the power of the cross-modulation product, while the last term (=5 dB) is added to account for the modulated nature of the TX [4]. For example, the integrated thermal noise is –101 dBm for 20-MHz channel bandwidth (BW) in an LTE RX. If we assume the cross-modulation product is equal to the noise power, i.e.,  $P_{XM} = -101$  dBm, the resulting required IIP3 is +36 dBm, which is a challenging specification that we will try to meet.

Fig. 2(b) shows some examples of LTE frequency bands. A single-switch  $RC$   $N$ -path filter [6] or mixer-first RX [1] performs “only” first-order low-pass filter (LPF), which is upconverted to a second-order bandpass filter (BPF) around the switching frequency. However, this is not sufficient to deal with strong TX leakage in the case of a very small “duplex spacing” [e.g., bands 5 and 8 in Fig. 2(b)].

To enhance the selectivity and extend the linearity, a sixth-order BPF was realized by cascading passive  $N$ -path filters, coupling them by transconductors  $g_m$  [7]. These transconductors work at RF in open loop and have a rather limited achievable linearity of around 10–15 dBm [8]. Even with a first passive stage [7], overall linearity was limited to +25 dBm, which is >10 dB worse than the +36 dBm requirement. Also, other  $g_mC$  filter techniques (see [9]) achieve good selectivity but insufficient linearity. An IIP3 = 36 dBm was demonstrated

Fig. 3. (a) Mixer-first RX with the BB Miller capacitor  $C_1$ . (b) Proposed RX with extra positive capacitive feedback.

by [5]; however, at a boosted switch-driver supply voltage of 2 V, raising power dissipation and introducing device reliability concerns. Recently, we proposed higher order RF filtering by cascading two passive BPF stages [10], while a “bottom-plate mixing” technique with switch sharing pushes IIP3 to +44 dBm. Unfortunately, large parasitic capacitance from method of moments capacitors at the RF input introduces signal loss, and sub-3-dB noise figure (NF) was not obtained.

In this paper, we propose a different approach to enhance selectivity in a mixer-first RX: we will exploit capacitive positive feedback to obtain a steeper filter roll-off [11], increased frequency range and enhanced linearity, while achieving an NF below 3 dB. Note that this is different from [3], where positive resistive (not capacitive) feedback is added to aid input impedance matching and realize sub-3-dB NF, whereas our key target is selectivity enhancement at high linearity. Compared to [11], this paper explains the concept in more depth, analyzes the filter transfer, NF, and stability, and adds some extra experimental results.

This paper is organized as follows. Section II introduces the architecture of the enhanced-selectivity mixer-first RX, while Section III proposes a circuit implementation. In Section IV, the RX performance is analyzed, especially, transfer function, loop stability, distortion, noise, and input impedance. Section V shows the measurement results and a performance comparison, while Section VI provides conclusions.

## II. RECEIVER ARCHITECTURE

To enhance IIP3 and compression point of the entire RX, strong OOB signals should be rejected as early as possible by steep filtering. This is what an SAW filter does, immediately at the RF input, but as motivated in the introduction, we would like a more CMOS compatible solution exploiting  $N$ -path filtering.

Fig. 3(a) shows a mixer-first RX, in which capacitor  $C_1$  is put across negative feedback amplifier  $-A_0$  and interacts with source impedance  $R_s$  via a passive mixer to obtain  $N$ -path filtering [1]–[3], [11]–[13]. The resulting first-order LPF is frequency shifted to a second-order RF BPF

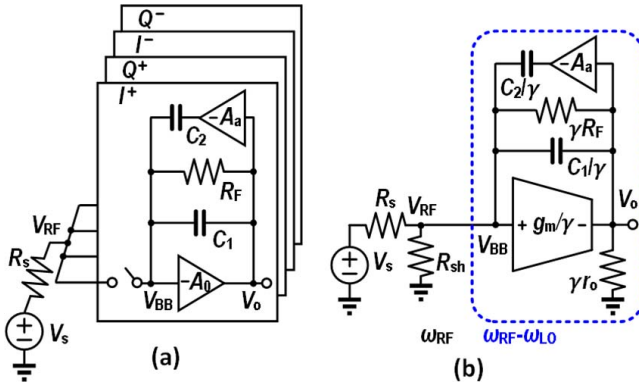


Fig. 4. (a) Four-phase case of the proposed RX. (b) Corresponding LTI model.

around  $f_{LO}$ . By putting  $C_1$  across the amplifier instead of to ground, the baseband (BB) capacitance “seen” by the mixer is increased due to the Miller effect by  $(1 + A_0)$ , saving chip area. Moreover, this Miller effect allows for low-noise impedance matching using a high  $R_F$  value [1]. A single-stage amplifier will be used, modelled as a voltage-controlled current source  $g_m$  with output resistance  $r_o$ , where  $A_0 = g_m r_o$ . Assuming  $r_o \ll R_F$ , an OOB blocker is downconverted and sees a BB conductance  $(Z_{BB})^{-1} \approx (Z_1)^{-1} + (1 + A_0)/R_F$ , with  $(Z_1)^{-1} \approx s(1 + A_o)C_1/(1 + sr_oC_1)$ . For frequencies  $\ll (r_oC_1)^{-1}$  and  $A_o \gg 1$ , conductance  $\approx (Z_1)^{-1}sA_oC_1$  offers OOB current bypassing and first-order filtering.

Higher order filtering can be obtained by creating a higher order input conductance, as shown in Fig. 3(b). A capacitive positive feedback path is added in the form of capacitor  $C_2$ , driven by the attenuated inverted BB signal, rendering

$$(Z_2)^{-1} \approx \frac{[s^2 r_o C_1 C_2 + s(1 - A_0 A_a) C_2]}{1 + sr_o C_1} \quad (2)$$

where  $A_0$  and  $A_a$  are positive numbers. The combination of negative feedback via  $C_1$  and positive feedback via  $C_2$  produces a two-zero, one-pole conductance, which can be approximated as

$$(Z_2)^{-1} + (Z_1)^{-1} \approx \frac{[s^2 r_o C_1 C_2 + s(1 - A_0 A_a) C_2 + sA_0 C_1]}{1 + sr_o C_1} \quad (3)$$

By choosing a proper  $A_a$  and  $C_1/C_2$  ratio, both zeros in (3) can be located at a frequency lower than  $(r_o C_1)^{-1}$ , and the conductance for a blocker offset frequency  $< (r_o C_1)^{-1}$  can be approximated as  $s^2 r_o C_1 C_2 + s(1 - A_0 A_a) C_2 + sA_0 C_1$ . This gives the approximations  $(Z_2)^{-1} \approx s^2 r_o C_1 C_2 + s(1 - A_0 A_a) C_2$  and  $(Z_1)^{-1} \approx sA_0 C_1$ , as shown in Fig. 3(b).

To get more detailed insights into the proposed mixer-first RX, we assume that four BB slices of the circuit in Fig. 3(b) are driven by four mixers and non-overlapping four-phase clocks with 25% duty cycle. The four-phase example of the proposed RX is shown in Fig. 4(a). We still assume that  $A_a$  is an ideal attenuator with infinite input impedance and zero output impedance. Adopting a derivation as in [14], we derived an equivalent linear time-invariant (LTI) model of the time-variant circuit and voltage transfer functions from the

RF signal  $V_s$  to the BB. The resulting LTI model for a sine wave RF excitation is shown in Fig. 4(b). (Note that the left part of the circuit operates at RF, and the right part at  $\omega_{BB} = \omega_{RF} - \omega_{LO}$  as in [14].) The harmonic shunt impedance  $R_{sh}$  of the passive mixer is  $4\gamma R_s/(1-4\gamma)$  [15]. Assuming ideal mixer switches, the voltage gain from  $V_{RF}$  to  $V_{BB}$  can be derived by dividing (4) in [15] by (6), resulting  $1/\sqrt{4\gamma}$  ( $= 0.9$  dB) where  $\gamma$  is  $2/\pi^2$  for the four-phase case. In our RX design,  $r_o$  is small because a large  $g_m$  is required for low noise.  $R_F$  is much higher than  $R_s$ , because  $R_F \approx R_s(1 + A_0)/(8\gamma - 1)$  is needed for input matching. We first show the single-ended to single-ended voltage transfer function  $H_{BB,S}(s) = V_{BB}(s)/(V_s/2)$ , and its natural frequency  $\omega_{0,S}$  and quality factor  $Q_S$

$$H_{BB,S}(s) = \frac{V_{BB}(s)}{V_s/2} \approx \frac{2\sqrt{4\gamma}((1 + A_a)C_2 4R_s)^{-1}(s + 1/(r_o C_1))}{s^2 + \frac{\omega_{0,S}}{Q_S} s + \omega_{0,S}^2} \quad (4)$$

$$\omega_{0,S} \approx \sqrt{\frac{1 + 4g_m r_o R_s R_F^{-1}}{4(1 + A_a)C_1 C_2 r_o R_s}} \quad (5)$$

$$Q_S \approx \frac{2\sqrt{(1 + A_a)C_1 C_2 r_o R_s (1 + 4g_m r_o R_s R_F^{-1})}}{4C_2(1 - A_a g_m r_o)R_s + C_1(r_o + 4R_s + 4g_m r_o R_s)} \quad (6)$$

When  $\omega_{BB} < 1/(r_o C_1)$ ,  $V_{BB}(s)/(V_s/2)$  is an LPF with two-pole roll-off. As  $\omega_{BB}$  increases to  $1/(r_o C_1)$ , this unwanted zero is introduced because the Miller capacitor  $C_1$  is no longer valid.

Next, we derive the  $H_{o,S}(s) = V_o(s)/(V_s/2)$ , and it can be written as

$$H_{o,S}(s) = \frac{V_o(s)}{V_s/2} \approx \frac{2\sqrt{4\gamma}((1 + A_a)C_2 4R_s)^{-1}\left(s - \frac{g_m}{C_1}\right)}{s^2 + \frac{\omega_{0,S}}{Q_S} s + \omega_{0,S}^2}. \quad (7)$$

The frequency of unwanted zero in  $H_{o,S}(s)$  that is located at  $g_m/C_1$  can be as high as 1 GHz if  $g_m$  is large enough. Then,  $H_{o,S}(s)$  effectively shows a two-pole roll-off below  $g_m/C_1$ . Fig. 5 compares the filter shape of a four-phase mixer-first RX with a BB Miller capacitor  $C_1$  in Fig. 3(a) and that of the new one with  $C_1$  and  $C_2$  in Fig. 3(b), designed as the Butterworth filter. Clearly, a more brick-wall like and also steeper RF BPF shape and BB LPF shape is achieved for blocker frequencies close to the RX-band compared to the “round shape” when cascading real poles.

We see that the combination of the new positive feedback path via  $C_2$  combined with the negative feedback path via  $C_1$  can establish a complex pole pair allowing to improve selectivity.

The quality factor  $Q$  is adjustable by changing the ratio of  $C_1$  and  $C_2$ . Note that both BB capacitive feedback paths can have high linearity as well as low noise, in contrast to open-loop  $g_m$  blocks. Before we analyze the practical circuit with non-ideal attenuator  $A_a$  in depth, we describe the actual circuit implementation in some more detail.

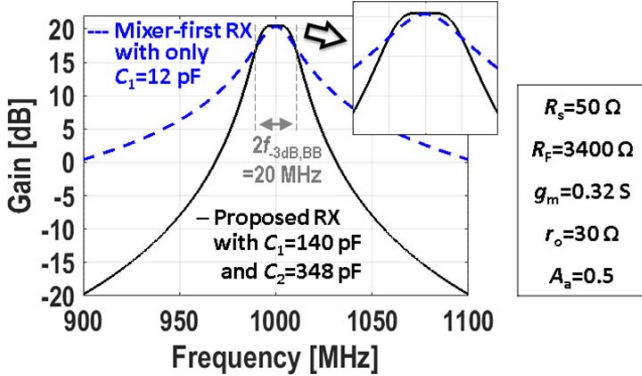


Fig. 5. Simulated (PXF)  $V_o(s)/(V_s/2)$  for the mixer-first RX with only  $C_1$  (dashed line) and the proposed mixer-first RX with  $C_1$  and  $C_2$  (solid line).  $C_1$  and  $C_2$  are tuned to have the same channel BW for fair comparison.

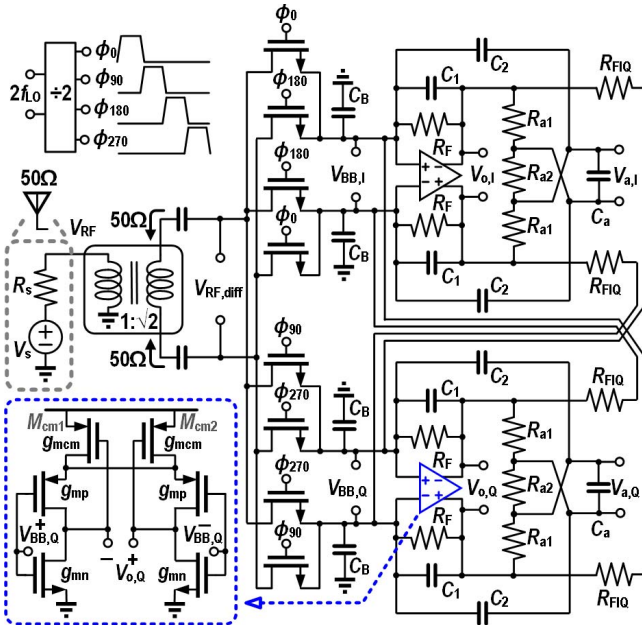


Fig. 6. Circuit details of the proposed RX and low-noise BB amplifier.

### III. CIRCUIT IMPLEMENTATION

Fig. 6 shows a detailed schematic of the proposed zero-IF RX. It was designed for  $f_{-3\text{ dB, BB}} = 10\text{ MHz}$  to support an RF channel bandwidth of 20 MHz for LTE applications. The passive mixer MOS switches are driven by quadrature four-phase 25% duty-cycle clocks, provided by a divide-by-2 circuit. Parasitic capacitance at the RF input causes the frequency of optimum  $S_{11}$  to shift toward lower frequencies than  $f_{\text{LO}}$ , which was compensated by complex feedback via  $R_{\text{FIQ}}$  [1].

#### A. Enhanced-Selectivity Receiver Circuit Realization

Due to the differential architecture, the negative gain  $-A_a$  for the attenuator in Fig. 6 can simply be implemented by wire crossing, while low-ohmic passive resistors  $R_{a1}$  and  $R_{a2}$  realize a high-linearity attenuator with  $A_a = 0.5$ . In Section IV, we will see that this hardly degrades NF. As  $C_2$  serves as OOB blocker bypassing path, low OOB impedance of the attenuator is important to maintain good blocker rejection. For this purpose capacitor  $C_a$  is added, providing a high-

linearity purely capacitive signal path shunting the BB input directly (see Fig. 6). The filter bandwidth is mainly determined by  $R_s$ ,  $C_1$ , and  $C_2$ , as will be derived in Section IV, and  $Q$  is designed about 0.7 to realize the Butterworth filtering. Capacitor  $C_B$  also provides a direct blocker bypassing path to ground but plays a minor role in this design, as the BB amplifier input impedance is low ohmic over a wideband due to the high  $g_m$  value used in this design (see below).

#### B. Low-Noise BB Amplifier

In the mixer-first RX, low noise in the first BB amplifier stage is an important requirement to achieve sub-3-dB RX NF. Inverter-based amplifiers [16], [17] offer large  $g_m$  with good power efficiency, while loop stability is of a little concern in a single-stage amplifier. Fig. 6 shows the schematic of the BB amplifier also used in [10]. A higher threshold voltage  $V_{\text{th}}$  for  $M_{\text{cm}1}$  and  $M_{\text{cm}2}$ , combined with a small overdrive voltage of the PMOS input differential pair ensures all transistors operate in their saturation region. The resistive attenuator in parallel to the MOS output resistance  $r_{\text{on}}$  and  $r_{\text{op}}$  linearizes the output impedance of the BB amplifier. For a differential input signal, a high gain of  $\approx(g_{mn} + g_{mp})(r_{\text{on}}||r_{\text{op}}) \approx 22\text{ dB}$  is achieved. For a pure common-mode input, the voltage gain  $g_{mn}/g_{mcn}$  is kept low as 5 dB. To avoid the kink or history effect in partially depleted silicon on insulator (SOI)-MOS transistors [18], the BB amplifiers were built by body-contacted devices, while mixer switches and digital clock generator devices are implemented as floating body devices. The dimensions of PMOS and NMOS input pairs are  $3600\text{ }\mu\text{m}/0.112\text{ }\mu\text{m}$  and  $1600\text{ }\mu\text{m}/0.112\text{ }\mu\text{m}$ , respectively, achieving a large  $g_m$  of  $360\text{ mS}$  and an output impedance  $r_o = r_{\text{on}}||r_{\text{op}} = 36\Omega$ . The simulated flicker noise corner frequency is about  $50\text{ kHz}$ , and the open-loop bandwidth is about  $340\text{ MHz}$  for a  $10\text{-pF}$  loading capacitance.

## IV. CIRCUIT ANALYSIS

In this section, we will analyze different properties of the mixer-first RX, such as transfer function, loop stability, linearity, noise, and input impedance.

#### A. Transfer Function Analysis

Using a similar derivation as in [14], we derived voltage transfer functions from  $V_s$  to  $V_{\text{BB,diff}}$ ,  $V_{o,\text{diff}}$ , and  $V_{a,\text{diff}}$  in Fig. 7. However, in contrast to a single-balanced mixer, we use a double-balanced mixer. Now each of the BB components is connected twice per period to the RF source, doubling the conduction time, compared to the single-end case. This leads to an equivalent LTI model with extra factors 2, as given in Fig. 7(a). The transformer with  $1:n$  turns ratio performs single-to-differential conversion. In this design, it is  $n = \sqrt{2}$  and impedance ratio is 1:2. To reduce equation complexity, we assume  $2R_{a1} = R_{a2} = R_a$  and neglect the minor effect of  $C_B$ . The pole and zero located at frequency higher than  $500\text{ MHz}$  are also neglected. We derived  $H_o(s) = V_{o,\text{diff}}(s)/(V_s/2)$ , its natural frequency  $\omega_0$  of the pole pair and quality factor  $Q$  as shown in (8)–(10) at the bottom of the next page. Since we consider now the finite gain of the BB amplifier, the equation becomes more complex than a normal

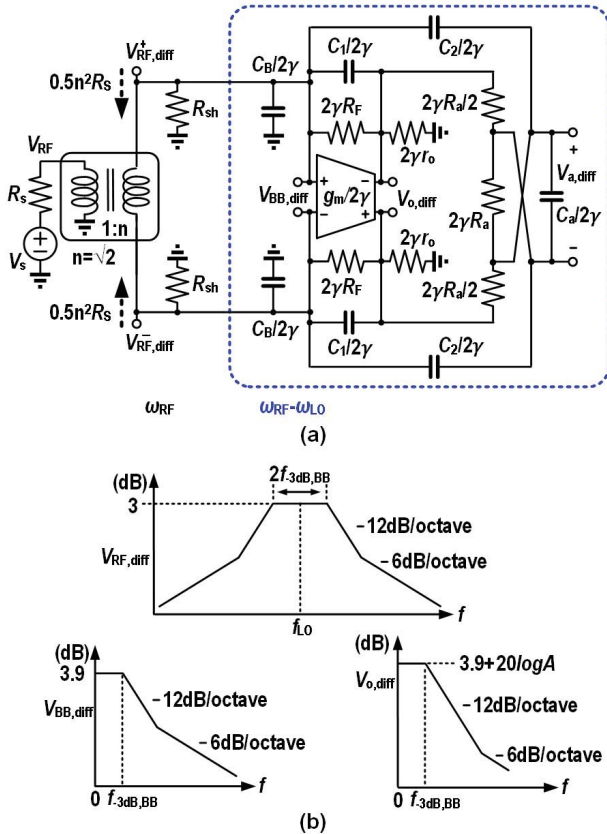


Fig. 7. (a) Equivalent LTI model of this RX. (b) Simplified plots for  $V_{RF,diff}$ ,  $V_{BB,diff}$ , and  $V_o,diff$ .

TABLE I  
COMPONENT VALUES FOR FIG. 7

$C_1=60$ pF	$C_a=120$ pF	$R_F=1600$ $\Omega$	$r_o=36$ $\Omega$
$C_2=106$ pF	$C_b=20$ pF	$R_s=90$ $\Omega$	$g_m=0.36$ S

biquad-transfer function. The resistive attenuator  $A_a$  instead of the uni-lateral block  $-A_a$  induces an unwanted left-half  $s$ -plane zero located at  $(0.5R_aC_a)^{-1}$ . It can be moved to higher frequency by using smaller attenuator resistance or  $C_a$ .

Filling in the component values listed in Table I, we find:  $\omega_0/2\pi = 9.5$  MHz, and a zero at 31 MHz. At  $\omega_0$ , the amplitude of  $H_o(s)$  is  $Q \cdot V_o,diff(0)/(V_s/2)$  so for a Butterworth filter

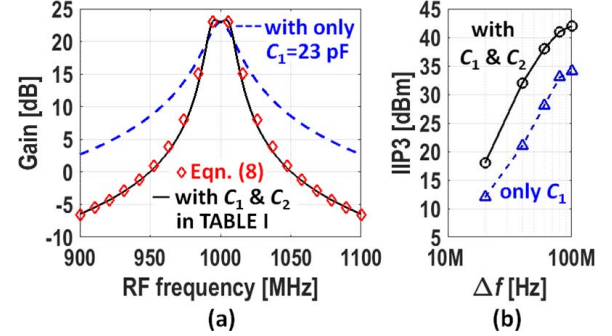


Fig. 8. (a) Simulated (PXF) and calculated (8) gain ( $V_o,diff(0)/(V_s/2)$ ) as a function of the RF frequency for the proposed mixer-first RX with  $C_1$  and  $C_2$  (solid line) and with only  $C_1$  (dashed line). (b) IIP3 simulation result for the same two cases.

$Q \approx 0.7$ ,  $\omega_0 = \omega_{BB,-3}$  dB. The simplified asymptotic plots of the transfer function to  $V_{RF,diff}$ ,  $V_{BB,diff}$ , and  $V_o,diff$  are shown in Fig. 7(b). The BB resistance  $R_F/(1+A)$  is upconverted and becomes  $2\gamma R_F/(1+A)$  at the RF input, where  $\gamma = 2/\pi^2$  for the four-path case [15] and  $A$  is  $g_m(r_o \parallel R_a \parallel R_F)$ . The upconverted BB resistance is in parallel with the harmonic shunt impedance  $R_{sh} = (0.5n^2 R_s)4\gamma/(1-4\gamma)$  of the passive mixer [15], where  $n$  is turns ratio of the transformer. The combined input impedance around the local oscillator (LO) frequency is  $R_{sh}/2\gamma R_F/(1+A)$  which is designed to provide 50- $\Omega$  matching. If there is in-band matching, in-band  $V_{RF}/(V_s/2)$  is 0 dB. Due to energy conservation,  $V_{RF,diff}/V_{RF}$  after the  $1:\sqrt{2}$  balun (100- $\Omega$  differentially) becomes +3 dB. The in-band voltage gain  $V_{BB,diff}/V_{RF}$  is  $\sqrt{2}(\sqrt{4\gamma})^{-1}$  corresponding to 3.9 dB. At the output of the BB amplifier  $V_o,diff$ , it is  $3.9 + 20\log A$  dB. For frequencies close to in-band, the roll-off is  $-12$  dB/octave. The output  $RC$  of the attenuator introduces a zero at 31 MHz, and hence, the slope degrades to  $-6$  dB/octave far out. Still, this steep roll-off part allows for better selectivity close to the desired band. Compared to the mixer-first RX with only the Miller capacitor  $C_1$ , simulations indeed show about 10-dB improvement in OOB IIP3 for the same mixer switch size, channel bandwidth and BB amplifier gain.

To verify analysis, Fig. 8(a) shows Spectre PSS PXF simulation results for the RX circuit schematic with ideal components. About 8 dB more OOB rejection at 45-MHz

$$H_o(s)$$

$$= \frac{V_o,diff(s)}{V_s/2} \approx -2\sqrt{2}\sqrt{4\gamma} \frac{2R_F/(1+g_m(r_o^{-1} + R_a^{-1} + R_F^{-1})^{-1})}{4R_s + 2R_F/(1+g_m(r_o^{-1} + R_a^{-1} + R_F^{-1})^{-1})} \frac{g_m(r_o^{-1} + R_a^{-1} + R_F^{-1})^{-1} \omega_0^2 (0.5R_aC_a s + 1)}{s^2 + \frac{\omega_0}{Q}s + \omega_0^2} \quad (8)$$

$$\omega_0^2 \approx \frac{2(r_o(R_F + 2R_s) + R_a(R_F + r_o + 2R_s + 2g_m r_o R_s))}{R_a(C_2 C_a (2R_F r_o + R_a(R_F + r_o)) 2R_s + C_1 R_F (6C_2 r_o R_s + C_a(4r_o R_s + R_a(r_o + 2R_s + 2g_m r_o R_s))))} \quad (9)$$

$$Q \approx \frac{\sqrt{(r_o R_F + R_a(R_F + 2g_m r_o R_s)) 2R_a (C_2 C_a (2R_F r_o + R_a R_F) 2R_s + C_1 R_F (6C_2 r_o R_s + 4C_a r_o R_s + 2C_a R_a g_m r_o R_s))}}{C_2 (3R_a r_o + 2R_F r_o + R_a R_F (2 - g_m r_o)) 2R_s + 2C_1 R_F (2r_o R_s + R_a(r_o + 2R_s + 2g_m r_o R_s)) + C_a R_a (2r_o R_F + R_a(R_F + 2g_m r_o R_s))} \quad (10)$$

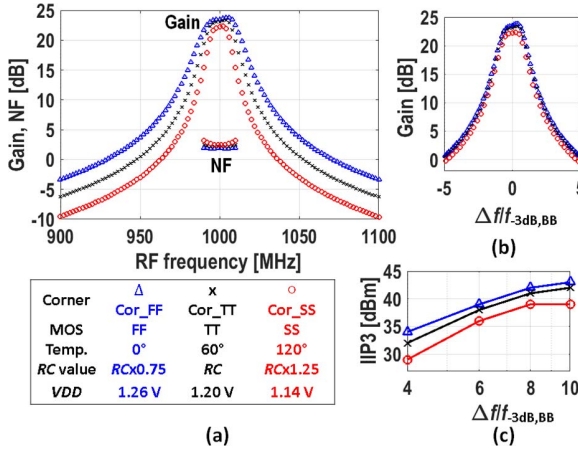


Fig. 9. PVT corner simulation results for (a) transfer function  $V_o/\text{diff}(0)/(V_s/2)$ , NF, (b) redrawn transfer function as a function of normalized frequency axis, and (c) IIP3.

duplex offset frequency (LTE-band 5) is found. The calculated transfer function (8) is also provided, where the BB frequency is shifted to the corresponding RF frequency and mixer conversion gain is taken into account. It shows a good fit with PSS simulations.

The IIP3 simulation results with transistor level Berkeley short-channel IGFET models (BSIMs) are provided in Fig. 8(b) to demonstrate that the extra filtering also results in extra overall IIP3 improvement. Since we experienced convergence issues using PSS simulations and there are effects of the discontinuity in the BSIM model, transient simulations with high accuracy settings and sufficiently high input power (-10 to +5 dBm) were applied to evaluate the IIP3. Intuitively, this makes sense, as the part of the waveform defined by the discontinuity becomes a smaller fraction of the total waveform. Overall, we found then a reasonable match (within 2–3 dB difference) between simulation and measurement.

The process, voltage, and temperature (PVT) variation simulation results for transfer function, NF, and IIP3 are shown in Fig. 9. The BPF bandwidth or  $\omega_0$  is controlled by  $RC$  value. The “filter shape” is determined by quality factor  $Q$  which is a function of  $R$ -to- $R$  and  $C$ -to- $C$  ratios; hence, it is insensitive to PVT variations. The frequency axis in Fig. 9(a) is shifted to BB frequency and normalized to  $f_{-3\text{dB},\text{BB}}$ . The RX transfer functions are redrawn and shown in Fig. 9(b) to confirm the robustness of RX selectivity against PVT variations. The simulated IIP3 as a function of relative frequency offset in Fig. 9(c) is kept within ≈3 dB variations while compared to the typical corner.

### B. Receiver Loop Stability

Positive feedback may introduce stability problems, so we will now analyze the feedback system loop gain  $H_{l,\text{diff}}(s)$ , i.e.,

$$H_{l,\text{diff}}(s) = [-A(s)] \cdot [-A_a(s)] \cdot \beta(s). \quad (11)$$

As the resistance of the attenuator is higher than  $r_o$ , the gain of the amplifier can be approximated as  $A(s) \approx A_0/(1+s r_o C_1)$ . The frequency-dependent gain of attenuator can be approximated as  $A_a(s) \approx A_a/(1+s(R_{a1}\parallel 0.5R_{a2})(2C_a+C_2))$ . It is a

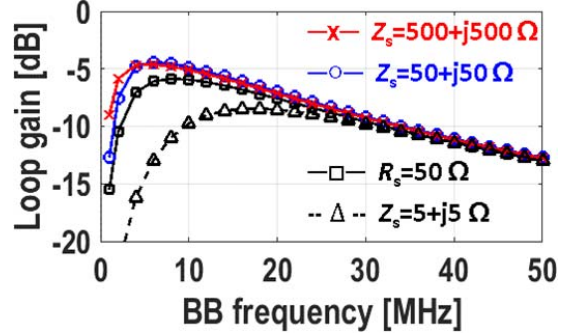


Fig. 10. Simulated differential loop gain for different antenna impedances  $Z_s$ .

low-pass function, and  $A_a = 1/2$ . Applying the Miller approximation, the feedback factor from attenuator output to the BB amplifier input is  $\beta(s) \approx s(C_2/C_1)/((R_s \parallel (A_0^{-1} R_F) C_1)^{-1} + s(C_2/C_1 + 1 + A_0))$ , which is a high-pass function. The positive loop gain  $H_{l,\text{diff}}(s)$  should be kept well below 0 dB to guarantee loop stability. At very low frequency,  $C_2$  provides a high impedance and  $\beta(0) \approx 0$ , so that  $H_{l,\text{diff}}(0) \approx 0$ . For increasing frequency, the impedance of  $C_1$  and  $C_2$  becomes lower resulting in lower  $A_0(s)$  and lower  $A_a(s)$  but higher  $\beta(s)$ . In this RX design,  $C_2 \approx 2C_1$ , resulting in  $H_{l,\text{diff}}(s) < A_0 A_a (C_2/C_1) / (C_2/C_1 + 1 + A_0) = A_0 / (3 + A_0) < 1$  for all frequencies. The resistive attenuator occupies a rather large area of  $20 \mu\text{m} \times 40 \mu\text{m}$  to prevent linearity degradation due to the voltage coefficient of poly-resistors, which also results in a good matching and an accurate resistor ratio  $A_a$ . Capacitance  $C_1$  and  $C_2$  are large, so  $C_2/C_1$  is also precise. The open loop gain of the BB amplifier  $A_0$  suffers more from process variation, but largely cancels in the ratio  $A_0/(3 + A_0)$  and reliably gives a value below 1. Therefore, loop stability is insensitive to PVT variations. Transistor-level Spectre PSS PSTB loop stability simulation shows  $H_{l,\text{diff}}(s)$  is < -6 dB for different transistors,  $R$ ,  $C$ , voltage, and temperature corners. The antenna impedance may change with user proximity in a mobile phone, and the antenna impedance  $Z_s$  may become more resistive and inductive [19]. Further analysis indicates that the proposed RX remains stable for different passive complex values of  $Z_s$ . As shown in Fig. 10, the simulated differential loop gain shows a BPF profile as predicted in (11), and is kept well below -4 dB (<0 dB for stable) for all frequencies even though there is  $10 \times Z_s$  variation. For common-mode signals, the wire crossing no longer results in a minus sign, and it becomes positive and unity gain. As a result, (11) changes to

$$H_{l,\text{CM}}(s) \approx \frac{-A_{0,\text{CM}}}{1+s r_o C_1} \frac{s C_2 / C_1}{((R_s \parallel (A_0^{-1} R_F) C_1)^{-1} + s(C_2/C_1 + 1 + A_0))}. \quad (12)$$

Hence, the common-mode loop gain  $H_{l,\text{CM}}(s)$  turns out to be negative feedback, in contrast to the differential loop gain  $H_{l,\text{diff}}(s)$ . Also, the single-stage BB amplifier (single-pole) is designed to have a low common-mode gain resulting in  $|H_{l,\text{CM}}(s)| < 1$ . Hence, there is no common-mode loop stability concern.

### C. OOB Linearity and OOB Rejection

The NMOS mixer switches suffer from modulated  $V_{GS}$  and  $V_{DS}$  that degrade the linearity of a mixer-first RX. Assuming that  $\rho = R_{sw}/R_s \ll 1$  (e.g.,  $\rho < 0.1$ ) to achieve high-linearity, in-band matching is mainly realized by  $R_F$ . For in-band, the  $V_{GS}$  modulation is  $\approx 0.5V_A$  and  $V_{DS}$  modulation is  $\approx 0.5V_A R_{sw}/R_s$  where  $V_A$  is the amplitude of the antenna source voltage. The in-band linearity of a mixer is dominated by large  $V_{GS}$  modulation. When the blocker offset frequency from the LO increases,  $V_{GS}$  modulation is reduced due to filtering. But  $V_{DS}$  modulation is slightly increased as the OOB current is higher than in-band. When the blocker is very far away from the LO frequency, the source terminal voltage swing of the mixer switch becomes almost zero, i.e.,  $V_{GS}$  modulation  $\approx 0$ . The modulated  $V_{DS}$  is  $\approx V_A R_{sw}/R_s$  and dominates the OOB linearity. The far OOB IIP3 can be estimated as [14]

$$V_{IIP3} = \sqrt{\frac{4}{3}} \frac{(1+\rho)^4}{\rho^3(2g_2^2 - g_3(1+\rho))} \quad (13)$$

where  $g_2$  is  $(2V_{OD})^{-1}$  and  $g_3 = -(2V_{SAT}^2)^{-1}$ .  $V_{OD}$  is overdrive voltage and  $V_{SAT}$  is velocity saturation voltage, respectively [14]. When the blockers are closed to the LO frequency, the proposed mixer-first RX with enhanced-RF selectivity achieves better OOB rejection and better linearity as the simulation results in Fig. 8 show.

To obtain extremely high OOB IIP3 of almost +40 dBm, high OOB linearity as well as high OOB rejection for both the mixer and the low noise BB amplifiers is demanded. The maximum OOB rejection of a mixer-first RX with a BB Miller capacitor that is shown in Fig. 3(a) is limited to  $\approx g_m^{-1}/R_s$  at the input of the BB amplifier. The OOB rejection can be extended by adding a capacitor  $C_B$  to the ground [1], [13]. However, for the same BW, a much larger capacitance area is required compared to  $C_1$ . Normally, there is a design tradeoff between linearity and maximum OOB rejection. The gain of the BB amplifier as a function of frequency can be expressed as  $A_o/(1 + A_o\beta(s))$ . The Miller capacitor  $C_1$  across the amplifier increases the feedback factor  $\beta(s)$  and improves the linearity of the BB amplifier at higher frequencies [20], while a BB amplifier without the Miller capacitor becomes linearity constraint in [13]. A high supply voltage of the BB amplifier can also result in better linearity [1], but consumes more power. Apart from the linearizing effect of the Miller capacitance, the output impedance of the BB amplifier is linearized by shunting it with the resistive attenuator. By adding  $C_a$ , we also directly shunt the BB amplifier input, avoiding the limited OOB rejection due to the finite  $g_m$  of BB amplifier. In the proposed mixer-first RX design, the maximum OOB rejection of the BB amplifier is improved compared to the mixer-first RX with BB Miller capacitors in Fig. 3(a), and the linearity of the BB amplifier is improved compared to [1] and [13].

### D. Noise Performance

The noise factor  $F$  of the RX can be calculated as the total output noise divided by the noise contribution due to

the thermal noise from the antenna or signal source, modelled as  $v_{n,s}^2 = 4kT R_s$ . The resulting  $F$  of this RX can be written as

$$\begin{aligned} F = 1 + \frac{R_{sw}}{R_s} + \frac{(R_s + R_{sw})}{4.3R_s} + \frac{(R_s + R_{sw})^2}{\gamma(2R_F)R_s} \\ + \frac{v_{n,in,A}^2(4(R_s + R_{sw}) + 2R_{BB})^2}{4kTR_s4\gamma(2R_{BB})^2} \\ + \frac{(r_o \| R_a)^2(4(R_s + R_{sw}) + 2R_{BB})^2}{A^2 R_a R_s 4\gamma(2R_{BB})^2}. \end{aligned} \quad (14)$$

The direct noise contribution from thermal noise of the mixer switch resistance which is in series with the source is  $R_{sw}/R_s$ . Moreover, noise degradation due to noise folding from odd harmonics of the mixer frequency occurs. Thermal noise of  $R_s$  and  $R_{sw}$  are hence downconverted [15], leading to a summation of  $4kT(R_s + R_{sw})/n^2$  terms, where  $n = 3, 5, 7, \dots$  for a four-path mixer. This sums up to  $\approx 4kT(R_s + R_{sw})/4.3$ . The upconverted noise current induced by the BB feedback resistor  $R_F$  renders the term proportional to  $1/(2\gamma R_F)$ , where  $\gamma$  is the scaling factor from [15] discussed in Section IV-A. Note that  $R_F$  is designed to provide 50-Ω matching, but it is much higher than  $R_s$  primarily due to the Miller effect. Therefore, the noise contribution of  $R_F$  is minor and it increases  $F$  by about only 0.08 in this design. The input-referred noise of the BB amplifiers  $v_{n,in,A}^2$  is  $v_{n,out,A}^2/A^2$ , where  $A = g_m(r_o \| R_a \| R_F)$  and  $v_{n,out,A}^2$  is noise at the BB amplifier output. The noise voltage due to source resistance at the BB amplifier input undergoes a voltage division with the gain of  $\sqrt{4\gamma}$ , and it is  $v_{n,s,BB}^2 = 4kTR_s(4\gamma)(2R_{BB}/(4(R_s + R_{sw}) + 2R_{BB}))^2$ , where  $R_{BB}$  is  $R_F/(1 + A)$ . The BB amplifier generates  $\sqrt{(v_{n,out,A}^2)} = 1400 \text{ pV}/\sqrt{\text{Hz}}$ , and the  $v_{n,in,A}^2/v_{n,s,BB}^2$  is low as 0.1 in this design. The last term in (14) comes from the resistive attenuator. The noise voltage is  $v_{n,att}^2 = 4kT(r_o \| R_a)^2/R_a$  where  $r_o$  is the output impedance of the MOS transistors. This contribution to  $F$  is only 0.006.

Equation (14) indicates that this RX design can achieve an NF of 1.6 dB ( $F = 1.46$ ) at low frequency with  $R_{sw} = 1.1 \Omega$ , where the harmonic folding term is the dominant one.

### E. Influence of Parasitic Capacitance at the RF Input Port

In a mixer-first RX or  $N$ -path filter, the optimum  $S_{11}$  (dip in  $S_{11}$ ) should be at  $\omega_{LO}$ . However, the parasitic capacitance  $C_p$  from the mixer switches, RF input pads, and tracks is in parallel with  $R_{in}(\omega_{LO}) = R_{sh}(\omega_{LO}) \| (\gamma 2R_{BB})$ , causing the frequency of optimum  $S_{11}$  to shift toward frequencies lower than  $\omega_{LO}$ . The total  $C_p$  is about 1 pF in this RX design. Assuming that  $R_s \gg R_{sw}$ , the input impedance around  $\omega_{LO}$  becomes

$$\begin{aligned} R_{in}(\omega_{LO}) \| (j\omega_{LO}C_p)^{-1} \\ = \frac{(R_{sh}(\omega_{LO}) \| (\gamma 2R_{BB})(1 - j\omega_{LO}(R_{sh}(\omega_{LO}) \| (\gamma 2R_{BB})C_p))}{1 + (\omega_{LO}(R_{sh}(\omega_{LO}) \| (\gamma 2R_{BB})C_p)^2}. \end{aligned} \quad (15)$$

Note that this is not a purely resistive impedance, but also contains a negative imaginary part, degrading  $S_{11}$ . Apart from

this (time-invariant) capacitor  $C_p$ , the impedance of the BB capacitance is upconverted, resulting in a positive imaginary part for frequencies below  $\omega_{\text{LO}}$ , but a negative inductance for frequencies above  $\omega_{\text{LO}}$  [15]. This latter effect can cancel the imaginary part of (15) at a frequency  $\omega_{\text{LO}} - \Delta\omega$  that is also roughly the frequency of optimum  $S_{11}$  due to  $C_p$ . To bring the dip of  $S_{11}$  back to  $\omega_{\text{LO}}$ , complex feedback with resistors  $R_{\text{FIQ}}$  can be applied [1]. The BB impedance  $jR_{\text{FIQ}}/A$  [15] is now upconverted with a scaling factor to cancel the term proportional to  $-j(\omega_{\text{LO}}C_p)^{-1}$  in (15). The required complex feedback resistance can be calculated as  $R_{\text{FIQ}} = A/(2\gamma\omega_{\text{LO}}C_p)$ , and lower resistance is demanded for the RX operating at higher frequency.  $R_{\text{FIQ}}$  also introduces a real part making the BB admittance  $Y_{\text{BB}} = (R_{\text{BB}})^{-1} = ((1+A)/RF + 1/R_{\text{FIQ}})$  is slightly higher ( $R_{\text{BB}}$  is lower). The  $C_p$  at RF input is in parallel with  $R_{\text{sh}}(\omega_{\text{LO}})$  that is composed of all odd harmonic shunt impedances in the four-path case.  $C_p$  decreases higher order harmonic shunt impedances and increases the folded noise. The  $R_{\text{sh}}(\omega_{\text{LO}})$  for a four-path mixer-first RX can be approximated as [14]

$$R_{\text{sh}}(\omega_{\text{LO}}) \approx 4.3R_{\text{sw}}(1 + (4R_{\text{sw}}C_p\omega_{\text{LO}} + R_{\text{sw}}/R_s)^{-1}). \quad (16)$$

At very low frequency,  $R_{\text{sw}} \approx 1.1 \Omega$  ( $W/L$  of an NMOS switch is  $300 \mu\text{m}/40 \mu\text{m}$ ),  $C_p \approx 1 \text{ pF}$  yields  $R_{\text{sh}}(0) = 4.3(R_s + R_{\text{sw}}) \approx 220 \Omega$ . At higher frequency that is  $\omega_{\text{LO}} = 2 \text{ GHz}$ ,  $R_{\text{sh}}(\omega_{\text{LO}})$  is reduced to  $68 \Omega$ , causing lower  $R_{\text{in}}(\omega_{\text{LO}}) = R_{\text{sh}}(\omega_{\text{LO}})\|(\gamma 2R_{\text{BB}}) = 33 \Omega$  and worse input matching. The RF input gain can be expressed as a voltage division of  $V_s R_{\text{in}}(\omega_{\text{LO}})/(R_s + R_{\text{in}}(\omega_{\text{LO}}))$ . The lower  $R_{\text{in}}(\omega_{\text{LO}})$  due to  $C_p$  also causes gain loss and can be computed as

$$\text{Gain loss at RF} = 20\log \left[ \left( \frac{R_{\text{in}}(\omega_{\text{LO}})}{R_s + R_{\text{in}}(\omega_{\text{LO}})} \right) / \left( \frac{R_{\text{in}}(0)}{R_s + R_{\text{in}}(0)} \right) \right]. \quad (17)$$

For example, the RF gain loss is about 2 dB at 2-GHz LO frequency. To compensate for the loss at RF, BB feedback resistance  $R_F$  can be adjusted to be higher to obtain higher upconverted resistance and bring the effective  $R_{\text{in}}(\omega_{\text{LO}})$  to  $50 \Omega$ . Both  $S_{11}$  degradation and gain loss at higher LO frequency can be compensated by  $R_F$  tuning. Note that it can be well compensated when  $R_{\text{sh}}(\omega_{\text{LO}}) > 50 \Omega$ . Unfortunately, the presence of  $C_p$  at the RF input still increasing the harmonic folding noise although the gain loss and  $S_{11}$  are compensated.

## V. MEASUREMENT RESULTS AND COMPARISON

This test chip has been fabricated in a GlobalFoundries 45-nm partially depleted SOI technology. A  $4 \times 4$  quad flat no-leads (QFN) package was used. The total area including pads and decoupling capacitors is  $1300 \mu\text{m} \times 1100 \mu\text{m}$ , while the active area is  $0.8 \text{ mm}^2$ . The highest aluminum layer covers almost the whole RX chip to provide very strong ground shielding. Fig. 11 shows the chip micrograph. The external differential clock is applied from the topside, while the RF input signal is applied from the bottom to minimize coupling. Wideband off-chip hybrids were used to serve as baluns to provide a differential RF signal and impedance match to the  $100-\Omega$  differential chip input. Both the hybrid and cable losses were de-embedded for all measurements.

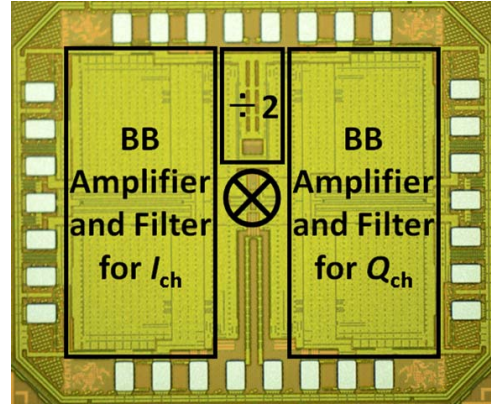


Fig. 11. Chip microphotograph.

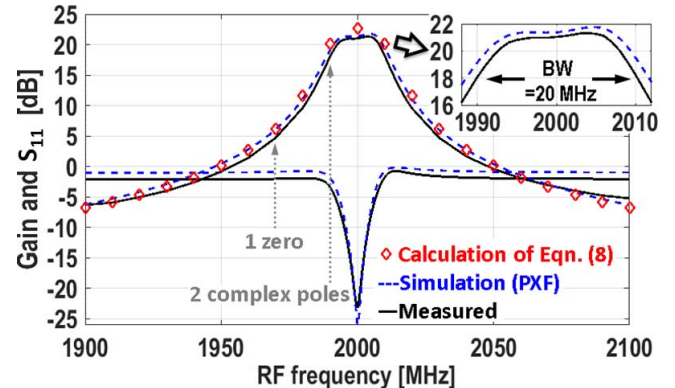


Fig. 12. Measured and simulated gain and  $S_{11}$  versus RF frequency ( $f_{\text{LO}} = 2 \text{ GHz}$ ). The calculated transfer function from (8) is also provided.

### A. Gain and $S_{11}$

Because the BB amplifier is not able to directly drive a  $50-\Omega$  load, a low-noise external measurement buffer with differential high-impedance input and single-ended  $50-\Omega$  output impedance was adopted. A weak tone of  $-50 \text{ dBm}$  is applied to the RF input, and the BB output is observed to obtain the conversion gain. Fig. 12 shows the measured and simulated gain and  $S_{11}$  as a function of the RF input frequency for a 2-GHz LO. The calculated transfer function from (8) is also provided. Both BB negative feedback and the complex-feedback resistors are programmed to compensate for the RF gain loss and  $S_{11}$  shifting due to parasitic capacitance at the RF input. The 21-dB gain and 20-MHz BPF channel bandwidth are obtained. As in simulation, the passband shows an asymmetrical slope induced by the complex feedback resistors. The peak of the gain roughly occurs at the middle between the center frequency and  $-3 \text{ dB}$  frequency, where the magnitude of the imaginary part of the input impedance is maximum. The  $jR_{\text{FIQ}}/A$  is upconverted to cancel the unwanted  $-j(\omega_{\text{LO}}C_p)^{-1}$  due to parasitic capacitance at the RF input, as discussed in Section IV-E. However, the gain of the BB amplifier  $A(s)$  is a function of frequency. Complete cancellation only happens at the exact center frequency. As the RF frequency changes, the residue  $-j/(\omega_{\text{LO}}C_p - A/(2\gamma R_{\text{FIQ}}))$  remains a negative imaginary impedance. The upconverted imaginary part of the BB impedance is positive for the low RF-sideband but negative for

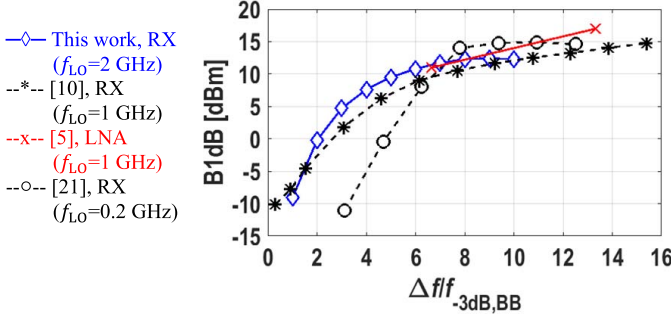


Fig. 13. Measured B1dB as a function of relative blocker frequency offset  $\Delta f/f_{-3\text{dB},\text{BB}}$  and comparison with other blocker-tolerant RF front ends.

the upper sideband [15]. The combination of these imaginary impedances results in an asymmetrical impedance profile at the RF input port. Together with passband ripple, this slope in the gain can be compensated in the digital domain. The complex poles are located at a BB frequency of 10 MHz. The measured filter roll-off is about 8.4 dB from 10- to 20-MHz offset frequency (it is 9.3 dB for an ideal Butterworth filter) and 8.2 dB from 20- to 40-MHz offset frequency. (It is 11.8 dB for an ideal Butterworth filter.) The less steep filter shape is due to a zero at a BB frequency of  $(2\pi \cdot 0.5R_aC_a)^{-1} = 31$  MHz that can be found in (8).

### B. B1dB, IIP2, and IIP3

To deal with a blocker that is closed to the RX-band is in general more difficult, as there are less octaves of filter suppression. Hence, it is preferable for fair benchmarking of linearity to consider the relative frequency offset normalized to the  $f_{-3\text{dB},\text{BB}}$ . Fig. 13 shows the measured B1dB as a function of  $\Delta f/f_{-3\text{dB},\text{BB}}$  for  $f_{\text{LO}} = 2$  GHz, and a desired signal is at 2.001 GHz ( $f_{\text{BB}} = 1$  MHz) for this work. Already at  $\Delta f/f_{-3\text{dB},\text{BB}} > 2$ , B1dB is  $> 0$  dBm, while for  $\Delta f/f_{-3\text{dB},\text{BB}} > 6$ , B1dB  $> +10$  dBm. Note that this design only uses a 1.2-V supply. (Other designs like [5] artificially boost B1dB by increasing the supply voltage introducing device reliability concerns.) The comparison with several blocker-tolerant RXs that achieved  $>+10$ -dBm B1dB [5], [10], [21] is also shown. A few decibel improvements for maximum B1dB can be achieved by adopting complementary MOS switches [21] or using the bottom-plate mixing technique proposed in [10] to realize more constant switch resistance. It also can be extended by applying higher supply voltage [5] at the cost of higher power consumption. Interestingly, the B1dB is improved by complementary switches but not IIP3 and input-referred second-order intercept point (IIP2). The bias point of the source and drain of both the PMOS and NMOS of a complementary switch is about  $V_{\text{DD}}/2$  in [21]. For this complementary switch design, the overdrive voltage is smaller than the designs with only NMOS switches [1], [3], [11], [13]. As a result, the switch resistance is higher leading to worse IIP3 and IIP2 [14]. Thanks to the steeper filter roll-off due to the complex pole pair in our design, we achieve a higher B1dB at lower relative frequency offset as shown in Fig. 13.

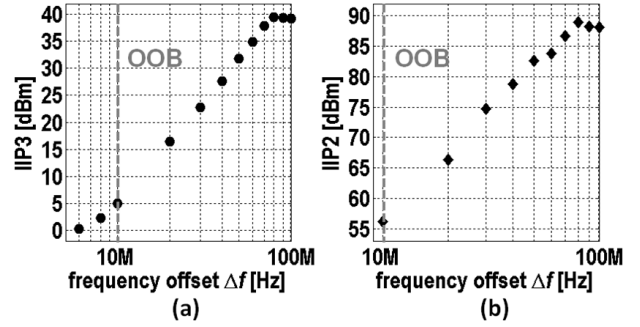


Fig. 14. Measured (a) IIP3 and (b) IIP2 versus blocker frequency offset  $\Delta f$  at  $f_{\text{LO}} = 2$  GHz.

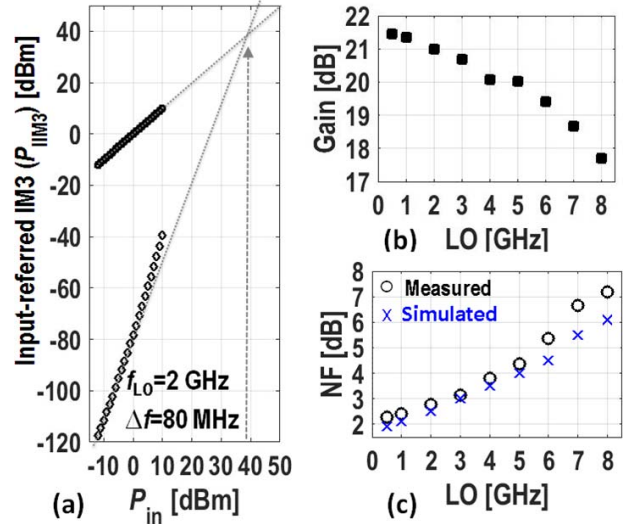


Fig. 15. (a) Measured  $P_{\text{IIM3}}$  versus  $P_{\text{in}}$  for  $\Delta f = 80$  MHz at  $f_{\text{LO}} = 2$  GHz, (b) measured gain and (c) DSB NF versus LO frequency. (PSS + PNOISE transistor-level simulated NF is also shown.)

IIP3 and IIP2 measurements are performed by two-tone tests. Circulators that offer higher than 20-dB isolation are applied between the two blocker signal generators to prevent intermodulation in the test setup, so that over +55 dBm IIP3 was achieved in the test setup itself. For LTE radio applications, the TX signal frequency is lower than the RX frequency for most of the bands. Therefore, the test tones were chosen at  $f_1 = f_{\text{LO}} - \Delta f$  and  $f_2 = f_{\text{LO}} - 2\Delta f + 500$  kHz for IIP3 measurements, and at  $f_1 = f_{\text{LO}} - \Delta f$  and  $f_2 = f_{\text{LO}} - \Delta f + 500$  kHz for IIP2 measurements. This choice keeps the resulting IM3 or IM2 product at a constant BB frequency of 500 kHz. Measured IIP3 and IIP2 as a function of  $\Delta f$  for a 2-GHz LO are shown in Fig. 14. At  $\Delta f = 80$  MHz, very high IIP3 of +39 dBm and IIP2 of +88 dBm are achieved. Fig. 15(a) shows the input-referred IM3 as a function of the blocker power for a 2-GHz LO and  $\Delta f = 80$  MHz. The measured  $P_{\text{IIM3}}$  follows that the extrapolation line up to an input power of 0 dBm and +39-dBm IIP3 is obtained.

### C. NF and Gain Versus LO Frequency

Measured gain as a function of LO frequency is shown in Fig. 15(b), and double sideband (DSB) NF is shown in Fig. 15(c). Measurement results show that the operating frequency can be up to 8 GHz, where an external clock

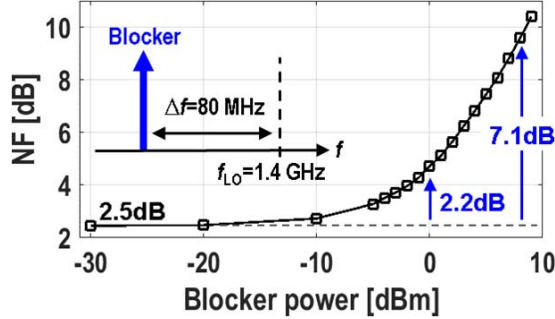


Fig. 16. Measured blocker NF for  $f_{LO} = 1.4$  GHz. (The highest  $f_{LO}$  for blocker NF measurement is 1.4 GHz due to the availability of external BPFs for blocker and clock sources.)

$2f_{LO} = 16$  GHz is applied. The limitation is the achievable rising and falling time of the inverter buffers that drive the mixer switches. It is a process-related parameter, where a more advanced technology achieves higher operating frequency. Measurement shows that the RX gain is kept within 1-dB degradation up to  $f_{LO} = 3$  GHz. NF measurements were performed using the Y-factor method with an external noise source. It is below 3 dB up to  $f_{LO} = 2$  GHz. The input parasitic capacitance due to mixer switches, input tracks, and pads is not taken into account in (14) of Section IV-D noise analysis. In the practical circuit, this lowers the impedance seen by the source voltage at higher RF frequencies. Therefore, the source resistance contributes a lower percentage of the total output noise at higher frequencies and NF increases. Also, lower complex feedback resistance is required to compensate for more  $S_{11}$  shifting at higher  $f_{LO}$  leading to more NF degradation (see also Section IV-E).

#### D. Blocker NF

A divide-by-two frequency divider is employed. The 25% duty-cycle LO pulses for quadrature mixing are obtained by combining the divider output with AND logical gates [1], [22]. In order to cover RF frequencies  $>6$  GHz and achieve low phase noise, the four-phase clock generator consumes 30 mW/GHz, targeting a phase noise of  $-171$  dBc/Hz at 80-MHz offset frequency (=duplexer offset). To ensure very low in-band noise of the blocker signal generator and low phase noise of the LO clock generator, two external tunable narrowband BPFs in cascade were applied to the output of the signal generators. This is done to ensure that the reciprocal mixing of the chip dominates performance, instead of phase noise from the measurement equipment. Fig. 16 shows the measured NF as a function of blocker power for 1.4-GHz LO, and blocker is 80 MHz from  $f_{LO}$ . Overall, the presence of strong blockers degrades NF due to reciprocal mixing and gain compression. Since the measured B1dB is as high as  $+12$  dBm, the blocker NF degradation is most likely due to reciprocal mixing. The measured desensitization is only 2.2 dB for a 0-dBm blocker, and 7.1 dB for an 8-dBm blocker. This design achieved a low 0-dBm blocker NF of 4.7 dB which is comparable to one of the best results published so far with a noise cancelling RX [17]. Note that, since an active  $g_m$  circuit is required at the RF input port for noise cancelling, linearity is limited in [17]. As a result, the achieved B1dB is

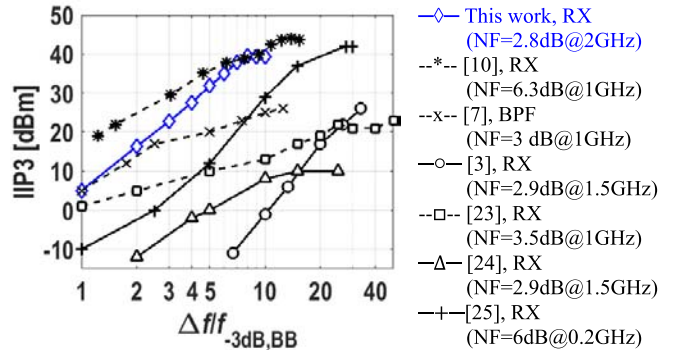


Fig. 17. IIP3 benchmark of blocker-tolerant RF front ends as a function of  $\Delta f/f_{-3\text{dB},\text{BB}}$ .

$<0$  dBm which causes blocker NF to degrade rapidly with higher blocker power ( $>10$  dB NF for  $+3$  dBm blocker). Thanks to the steeper filter roll-off due to complex poles at the RF input that reject blockers, this design maintains a blocker NF  $<10$  dB up to an  $+8$  dBm blocker.

#### E. Performance Comparison

Fig. 17 shows an IIP3 benchmark of blocker-tolerant RF front ends as a function of  $\Delta f/f_{-3\text{dB},\text{BB}}$ . Circuit type, NF, and operating frequency are also indicated. This design achieves high linearity while keeping NF  $<3$  dB. Note that the RX design in [10] which is also proposed by us achieved higher linearity but limited operating frequency and significantly higher NF. A performance summary and comparison are shown in Table II. Compared to the prior art, the RX achieves high IIP3, IIP2, and wider operating frequency  $f_{RF}$ , while maintaining comparable NF and power consumption. This confirms that the effectiveness of the higher RF BPF selectivity provided by the proposed mixer-first RX exploiting positive capacitive feedback.

#### F. LTE-Band 5 Diversity Antenna Path Experiment

Fig. 18 shows a test setup used to evaluate the sensitivity for an LTE-band 5 scenario. The TX frequency is 824–849 MHz, and the RX frequency is 869–894 MHz, i.e., 45-MHz duplex spacing. An in-band signal at the RX-band (880 MHz) plus 1.7-MHz offset is applied to the RX port of the triplexer. A 20-MHz BW modulated signal is applied at 835 MHz to the TX port, and a CW blocker is applied to the BLK port at 790 MHz. The triplexer implements BPF and combines the three signals, and the sum is connected to the main antenna of an actual cell phone antenna via an SMA connector. There is about 15-dB isolation between the main and diversity antennas. The diversity antenna path of this cell phone is connected to this RX chip for a sensitivity test. Assuming that the noise floor is  $KT$  at the antenna, the NF is obtained by observing the SNR degradation at the RX output. The external measurement buffer amplifier was used again, and an LPF filter is added at the external buffer output to prevent the corruption of the spectrum analyzer performance due to strong downconverted TX signals. The hybrid and cable loss as well as the external buffer and spectrum analyzer noise were deembedded. Fig. 19 shows the measured RX NF as a function

TABLE II  
RESULT SUMMARY AND COMPARISON WITH PRIOR ARTS

	JSSC10[1]	JSSC12[17]	JSSC13[7]	JSSC15[9]	RFIC15[2]	RFIC15[3]	RFIC15[5]	ISSCC17[10]	This Work
Architecture	Mixer first	Mixer first with Noise Cancelling	N-path filter	Mixer first +2 <sup>nd</sup> order baseband	Mixer first with LO leakage suppression	Mixer first with positive resistive feedback	Feedback with N-path filter	N-path filters with bottom -plate mixing	Mixer first with positive capacitive feedback
Circuit type	Receiver	Receiver	LNA/Filter	Receiver	Receiver	Receiver	LNA/Filter	Receiver	Receiver
Technology	65nm	40nm	65nm	65nm	28nm	65nm	32nm SOI	28nm	45nm SOI
$f_{RF}[\text{GHz}]$	0.1-2.4	0.08-2.7	0.1-1.2	0.5-3	0.4-3.5	0.7-3.8	0.4-6	0.1-2.0	0.2-8
Gain[dB]	40-70	72	25	50	35	40	12	16	21
BB BW[MHz]	10	2	4	1-30	15-50	3	7.5	6.5	10
OOB IIP3[dBm]	25 $\Delta f/\text{BW} = 10$	13.5 $\Delta f/\text{BW} = 40$	26 $\Delta f/\text{BW} = 12.5$	-4.8 $\Delta f/\text{BW} = 8$	20.5 $\Delta f/\text{BW} = 3.3$	26 $\Delta f/\text{BW} = 33.3$	36 $\Delta f/\text{BW} = 6.7$	44 $\Delta f/\text{BW} = 12.3$	39 $\Delta f/\text{BW} = 8$
OOB IIP2[dBm]	56	55	NA	NA	64	65	NA	90	88
B1dB[dBm]	10 $\Delta f/\text{BW} = 10$	-2 $\Delta f/\text{BW} = 40$	7 $\Delta f/\text{BW} = 12.5$	-10 $\Delta f/\text{BW} = 8$	4.6 $\Delta f/\text{BW} = 3.3$	3 $\Delta f/\text{BW} = 33.3$	>17 $\Delta f/\text{BW} = 13.3$	13 $\Delta f/\text{BW} = 12.3$	12 $\Delta f/\text{BW} = 8$
NF[dB]	$4 \pm 1$ (2GHz $f_{LO}$ )	1.9	2.8	3.8-4.7	2.4-2.6	2.5-4.5	3.6-4.9	6.3 (1GHz $f_{LO}$ )	2.3-5.4 (0.5-6GHz $f_{LO}$ )
0dBm Blocker NF[dB]	NA	4.1 ( $f_{LO}=1.5\text{GHz}$ )	NA	NA	6.5 ( $f_{LO}=2\text{GHz}$ )	NA	NA	8.1 ( $f_{LO}=1.3\text{GHz}$ )	4.7 ( $f_{LO}=1.4\text{GHz}$ )
LO leakage [dBm]	-65 ( $f_{LO}=1\text{GHz}$ )	NA	<-64 ( $f_{LO}=1\text{GHz}$ )	NA	<-62	<-60	<-40	NA	<-65
Supply[V]	1.2/2.5	1.2/2.5	1.2	1.2/2.5	1/1.5	1.2	2	1.2/1.0	1.2
Power[mW]	37-70	27-60	15-48	RX:76-168 LO:54-194	38-75	27-75	81-209	38-96	50mW*+ 30mW/GHz**
Area[mm <sup>2</sup> ]	2.5	1.2	0.27	7.8	0.23	0.23	0.28	0.49	0.8

\*power consumption of BB amplifiers = 50 mW, \*\*clock generator power is 30 mW/GHz.

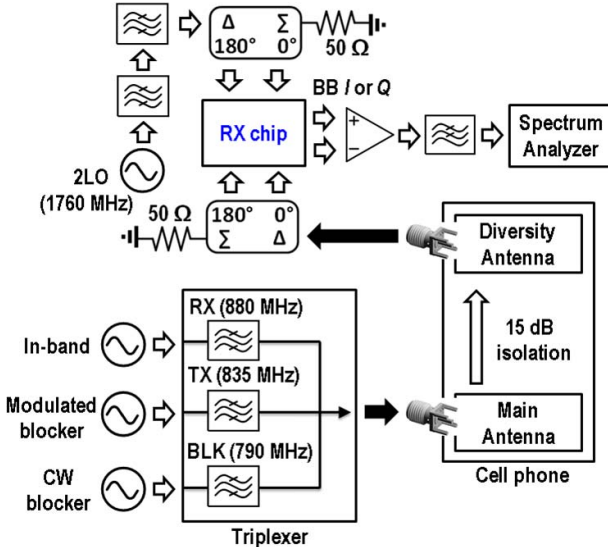


Fig. 18. LTE-band 5 sensitivity test setup.

of TX power. The measured NF is about 4.7 dB at very low TX power, while the measured NF using the Y-factor method in Fig. 15(c) is about 2.5 dB. This is because the antenna only provides the RX with an in-band 50- $\Omega$  impedance matching, while there is wideband 50- $\Omega$  impedance for the external noise source used in the Y-factor NF measurement. The lower harmonic shunt impedance generates more noise current bringing,

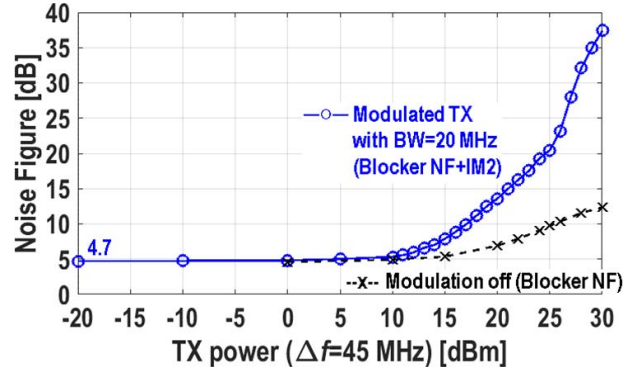


Fig. 19. Measured diversity RX NF as a function of TX power.

leading to higher NF. First, we measured the NF when the TX modulation is OFF and the TX produces a single tone at 835 MHz. This corresponds to a blocker NF measurement. The measured desensitization is only 0.7 dB for a 15-dBm blocker and 4.4 dB for 24-dBm blocker. Next, the TX modulation is turned on and the IM2 increases the noise floor. The measured desensitization due to IM2 and reciprocal mixing is about 3 dB when the TX power is +15 dBm. If the TX power is higher than +25 dBm, the NF deteriorates rapidly since the TX leakage power to diversity RX is higher than B1dB and gain compression worsens the NF as well. A -15 dBm CW blocker at 790 MHz is also fed to the BLK port for IIP3 desensitization tests. Since there is about 15-dB isolation, the actual CW

blocker at the diversity RX is about  $-30$  dBm. The noise floor induced by IM3 in a certain BW can be calculated as  $N_{IM3} = 3P_{in} - 2 \cdot IIP3 - 10\log(BW)$  when TX power is equal to CW blocker power. The IIP3 is about  $+30$  dBm at 45-MHz duplexer frequency in this design. For a  $P_{in} = 30$  dBm, RF channel BW of 20 MHz,  $N_{IM3}$  is about  $-220$  dBm/Hz which is much lower than  $KT$ ; therefore, the IIP3 induced desensitization was not detectable.

## VI. CONCLUSION

In this paper, a mixer-first RX with enhanced selectivity due to capacitive positive feedback was proposed. It improves the filter shape exploiting a complex pole pair, while achieving sub-3-dB NF and high linearity ( $IIP3 > 36$  dBm and  $B1dB > 10$  dBm) as required for LTE FDD diversity RXs. Important RX properties were analyzed, like filter shape in terms of natural frequency  $\omega_0$ , quality factor  $Q$ , bandwidth, and NF. To evaluate stability, the loop gain as a function of frequency was related to the amplifier gain, attenuator transfer, and the capacitor ratio of two feedback paths. Loop gain is reliably kept below  $-6$  dB, and the loop stability is insensitive to PVT and antenna impedance variations. This RX design covers all sub-6-GHz cellular bands and achieves a high IIP3 of  $+39$  dBm, IIP2 of  $+88$  dBm, and blocker 1-dB gain compression point of  $+12$  dBm for a blocker frequency offset of 80 MHz at 2-GHz LO while achieving an NF of 2.8 dB. The measured NF ranges from 2.4 dB at  $f_{LO} = 1$  GHz to 5.4 dB at  $f_{LO} = 6$  GHz. The measured desensitization is only 2.2 dB for 0-dBm blocker and 7.1 dB for 8-dBm blocker, demonstrating robustness to TX leakage and strong blockers.

## ACKNOWLEDGMENT

The authors would like to thank G. Wienk for CAD assistance and H. de Vries for help during measurements. They would also like to thank GlobalFoundries, USA, for supporting the chip fabrication.

## REFERENCES

- [1] C. Andrews and A. C. Molnar, "A passive mixer-first receiver with digitally controlled and widely tunable RF interface," *IEEE J. Solid-State Circuits*, vol. 45, no. 12, pp. 2696–2708, Dec. 2010.
- [2] C. Wu, Y. Wang, B. Nikolic, and C. Hull, "A passive-mixer-first receiver with LO leakage suppression, 2.6 dB NF,  $>15$  dBm wide-band IIP3, 66 dB IRR supporting non-contiguous carrier aggregation," in *Proc. IEEE Radio Freq. Integr. Circuits Symp.*, May 2015, pp. 155–158.
- [3] A. Nejdel, M. Abdulaziz, M. Törmänen, and H. Sjöland, "A positive feedback passive mixer-first receiver front-end," in *Proc. IEEE Radio Freq. Integr. Circuits Symp.*, Jun. 2015, pp. 79–82.
- [4] V. Aparin and L. E. Larson, "Analysis and reduction of cross-modulation distortion in CDMA receivers," *IEEE Trans. Microw. Theory Techn.*, vol. 51, no. 5, pp. 1591–1602, May 2003.
- [5] C.-K. Luo, P. S. Gudem, and J. F. Buckwalter, "0.4–6 GHz, 17-dBm B1dB, 36-dBm IIP3 channel-selecting, low-noise amplifier for SAW-less 3G/4G FDD receivers," in *Proc. IEEE Radio Freq. Integr. Circuits Symp.*, Jun. 2015, pp. 299–302.
- [6] A. Ghaffari, E. A. M. Klumperink, M. C. M. Soer, and B. Nauta, "Tunable high- $Q$  N-path band-pass filters: Modeling and verification," *IEEE J. Solid-State Circuits*, vol. 46, no. 5, pp. 998–1010, May 2011.
- [7] M. Darvishi, R. van der Zee, and B. Nauta, "Design of active N-path filters," *IEEE J. Solid-State Circuits*, vol. 48, no. 12, pp. 2962–2976, Dec. 2013.
- [8] H. K. Subramaniyan, E. A. M. Klumperink, V. Srinivasan, A. Kiaei, and B. Nauta, "RF transconductor linearization robust to process, voltage and temperature variations," *IEEE J. Solid-State Circuits*, vol. 50, no. 11, pp. 2591–2602, Nov. 2015.
- [9] R. Chen and H. Hashemi, "Dual-carrier aggregation receiver with reconfigurable front-end RF signal conditioning," *IEEE J. Solid-State Circuits*, vol. 50, no. 8, pp. 1874–1888, Aug. 2015.
- [10] Y. Lien, E. Klumperink, B. Tenbroek, J. Strange, and B. Nauta, "A high-linearity CMOS receiver achieving +44 dBm IIP3 and +13 dBm B1dB for SAW-less LTE radio," in *IEEE ISSCC Dig. Tech Papers*, Feb. 2017, pp. 412–413.
- [11] Y. Lien, E. Klumperink, B. Tenbroek, J. Strange, and B. Nauta, "A mixer-first receiver with enhanced selectivity by capacitive positive feedback achieving +39 dBm IIP3 and <3 dB noise figure for SAW-less LTE radio," in *Proc. IEEE Radio Freq. Integr. Circuits Symp.*, Jun. 2017, pp. 280–283.
- [12] E. A. M. Klumperink, H. J. Westerveld, and B. Nauta, "N-path filters and mixer-first receivers: A review," in *Proc. IEEE Custom Integr. Circuits Conf. (CICC)*, Austin, TX, USA, Apr./May 2017, pp. 1–8.
- [13] M. C. M. Soer, E. A. M. Klumperink, Z. Ru, F. E. van Vliet, and B. Nauta, "A 0.2-to-2.0 GHz 65 nm CMOS receiver without LNA achieving  $\gg 11$  dBm IIP3 and  $\ll 6.5$  dB NF," in *IEEE ISSCC Dig. Tech Papers*, Feb. 2009, pp. 222–223 and 223a.
- [14] D. Yang, C. Andrews, and A. Molnar, "Optimized design of N-phase passive mixer-first receivers in wideband operation," *IEEE Trans. Circuits Syst. I, Reg. Papers*, vol. 62, no. 11, pp. 2759–2770, Nov. 2015.
- [15] C. Andrews and A. C. Molnar, "Implications of passive mixer transparency for impedance matching and noise figure in passive mixer-first receivers," *IEEE Trans. Circuits Syst. I, Reg. Papers*, vol. 57, no. 12, pp. 3092–3103, Dec. 2010.
- [16] B. Nauta, "A CMOS transconductance-C filter technique for very high frequencies," *IEEE J. Solid-State Circuits*, vol. 27, no. 2, pp. 142–153, Feb. 1992.
- [17] D. Murphy *et al.*, "A blocker-tolerant, noise-cancelling receiver suitable for wideband wireless applications," *IEEE J. Solid-State Circuits*, vol. 47, no. 12, pp. 2943–2963, Dec. 2012.
- [18] S. Krishnan, J. G. Fossum, P. C. Yeh, O. Faynot, S. Cristoloveanu, and J. Gautier, "Floating-body kinks and dynamic effects in fully depleted SOI MOSFETs," in *Proc. IEEE Int. SOI Conf.*, Oct. 1995, pp. 10–11.
- [19] K. R. Boyle, Y. Yuan, and L. P. Lighthart, "Analysis of mobile phone antenna impedance variations with user proximity," *IEEE Trans. Antennas Propag.*, vol. 55, no. 2, pp. 364–372, Feb. 2007.
- [20] W. Sansen, "Distortion in elementary transistor circuits," *IEEE Trans. Circuits Syst. II, Exp. Briefs*, vol. 46, no. 3, pp. 315–325, Mar. 1999.
- [21] Y. Xu and P. R. Kinget, "A switched-capacitor RF front end with embedded programmable high-order filtering," *IEEE J. Solid-State Circuits*, vol. 51, no. 5, pp. 1154–1167, May 2016.
- [22] A. Mirzaei, H. Darabi, J. C. Leete, and Y. Chang, "Analysis and optimization of direct-conversion receivers with 25% duty-cycle current-driven passive mixers," *IEEE Trans. Circuits Syst. I, Reg. Papers*, vol. 57, no. 9, pp. 2353–2366, Sep. 2010.
- [23] H. Hedayati, V. Aparin, and K. Entesari, "A +22 dBm IIP3 and 3.5 dB NF wideband receiver with RF and baseband blocker filtering techniques," in *Symp. VLSI Circuits Dig. Tech. Papers.*, Jun. 2014, pp. 36–37.
- [24] Z. Lin, P.-L. Mak, and R. P. Martins, "A  $0.028 \text{ mm}^2$  11 mW single-mixing blocker-tolerant receiver with double-RF N-path filtering,  $S_{11}$  centering, +13 dBm OB-IIP3 and 1.5-to-2.9 dB NF," in *IEEE ISSCC Dig. Tech. Papers*, Feb. 2015, pp. 36–37.
- [25] H. Westerveld, E. Klumperink, and B. Nauta, "A cross-coupled switch-RC mixer-first technique achieving +41 dBm out-of-band IIP3," in *Proc. IEEE Radio Freq. Integr. Circuits Symp.*, Jun. 2016, pp. 246–249.

**Yuan-Ching Lien (S'16)** was born in Taipei, Taiwan. He received the B.S. and M.S. degrees in electrical engineering from National Taiwan University, Taipei, Taiwan.

In 2007, he joined MediaTek Inc., Hsinchu, Taiwan. From 2014 to 2018, he was a Ph.D. Researcher with the University of Twente, Enschede, The Netherlands. His current research interests include continuous-time filters, Nyquist-rate data converters, and reconfigurable RF front ends.





**Eric A. M. Klumperink** (M'98–SM'06) was born in Lichtenvoorde, The Netherlands, in 1960. He received the B.Sc. degree from HTS, Enschede, The Netherlands, in 1982. His Ph.D. dissertation was “Transconductance Based CMOS Circuits” in 1997.

He was with industry where he was involved in digital hardware and software, and then he joined the University of Twente, Enschede, in 1984, where he was involved in analog CMOS circuit research. In 1998, he became an Assistant Professor with the IC-Design Laboratory, University of Twente, and shifted research focus to RF CMOS circuits (e.g., sabbatical at the Ruhr Universitaet, Bochum, Germany). Since 2006, he has been an Associate Professor with the IC Design Group, University of Twente, teaching analog and RF IC electronics and guiding Ph.D. and M.Sc. projects related to RF CMOS circuit design with a focus on software defined radio, cognitive radio, and beamforming. He has authored or co-authored over 150 internationally refereed journal and conference papers, and was recognized as one of the Over-20 ISSCC Papers Contributors from 1954 to 2013. He holds several patents.

Dr. Klumperink was a co-recipient of 2002 and 2009 Van Vessel Outstanding Paper Award. He served as an Associate Editor for the IEEE TCAS-II from 2006 to 2007, the IEEE TCAS-I from 2008 to 2009, and the IEEE JOURNAL OF SOLID-STATE CIRCUITS from 2010 to 2014, and as an IEEE SSC Distinguished Lecturer from 2014 to 2015. He was a member of the technical program committees of the IEEE International Solid-State Circuits Conference from 2011 to 2016 and has been a member of the IEEE RFIC Symposium since 2011.



**Bernard Tenbroek** received the M.Sc. degree in electrical engineering from the University of Twente, Enschede, The Netherlands, in 1993, and the Ph.D. degree from the University of Southampton, Southampton, U.K., in 1997.

From 1997 to 1998, he was a Research Fellow with the University of Southampton. From 1998 to 2000, he was a Staff Engineer with Asahi Kasei Microelectronics. From 2000 to 2008, he was a Design Manager with Analog Devices. In 2008, he joined MediaTek as a Design Engineering Manager at the MediaTek RF Design Center, U.K., where he was involved in advanced cellular transceivers. He has authored over 20 journal and conference papers, and holds two patents.

Dr. Tenbroek was a recipient of the ISSCC Outstanding European Paper Award in 2007.



**Jon Strange** (M'00–SM'11) was born in Wigan, U.K., in 1963. He received the B.Sc. degree in physics from the University of Durham, Durham, U.K., in 1984, and the M.Sc. degree in microelectronics from the University of Edinburgh, Edinburgh, U.K., in 1985.

From 1985 to 1987, he was a Researcher with the VLSI Department, Thorn-EMI Central Research Laboratories, and from 1988 to 1991, he held several design and engineering management positions for large-scale integrated logic. In 1991, he cofounded

Mosaic Micro Systems, Ltd., an RF and wireless design consultancy specializing in the RF and radio system IC design which was acquired by analog devices in 1996. From 1996 to 2008, he was an Engineering Director with the RF and Wireless Business Unit Analog Devices Inc., responsible for the RF IC product design. He is currently a Senior Director of RF Design and a fellow with Mediatek Wireless Ltd., Kent, U.K., where he is responsible for developing cellular transceivers and related technologies for mobile platforms. He has authored or co-authored 15 technical conference and journal papers. He holds 16 granted U.S. patents.



**Bram Nauta** (S'89–M'91–SM'03–F'08) was born in Hengelo, The Netherlands, in 1964. He received the M.Sc. degree (*cum laude*) in electrical engineering, and the Ph.D. degree in analog CMOS filters for very high frequencies from the University of Twente, Enschede, The Netherlands, in 1987 and 1991, respectively.

In 1991, he joined the Mixed-Signal Circuits and Systems Department of Philips Research, Eindhoven, The Netherlands. In 1998, he returned to the University of Twente, where he is currently a Distinguished Professor, heading the IC Design Group. Since 2016, he has been serving as Chair with the Electrical Engineering Department, University of Twente. His current research interest include high-speed analog CMOS circuits, software defined radio, cognitive radio, and beamforming.

Dr. Nauta was a co-recipient of the ISSCC 2002 and 2009 Van Vessem Outstanding Paper Award. He received the Simon Stevin Meester Award (500.000€) in 2014, the largest Dutch national prize for achievements in technical sciences. He served as the Editor-in-Chief from 2007 to 2010 for the IEEE JOURNAL OF SOLID-STATE CIRCUITS (JSSC), and was the 2013 Program Chair of the IEEE International Solid-State Circuits Conference (ISSCC). He is the President of the IEEE Solid-State Circuits Society for the term 2018 to 2019. Also, he served as an Associate Editor for the IEEE TRANSACTIONS ON CIRCUITS AND SYSTEMS II from 1997 to 1999 and for JSSC from 2001 to 2006. He was on the Technical Program Committee of the Symposium on VLSI Circuits from 2009 to 2013. He is on the Steering Committee and Program Committee of the European Solid-State Circuit Conference (ESSCIRC). He has served as a Distinguished Lecturer for the IEEE. He is a member of the Royal Netherlands Academy of Arts and Sciences.